Characterization and parametrization in terms of atomic number of x-ray emission from *K*-shell filling during ion-surface interactions

S. J. McMahon,[1] A. P. Kavanagh,[2] H. Watanabe,[3] J. Sun,[3] M. Tona,[4] N. Nakamura,[5] S. Ohtani,[5] and F. J. Currell[1]

[1]*Centre for Plasma Physics, School of Mathematics and Physics, Queen's University Belfast, Belfast, BT7 1NN, Northern Ireland, United Kingdom*

[2]*Royal Marsden NHS Foundation Trust and Institute of Cancer Research, London, United Kingdom*

[3]*Chubu University, Kasugai, Aichi 487-8501, Japan*

[4]*Department of Chemistry, Kobe University, Kobe, Hyogo 657-8501, Japan*

[5]*Institute for Laser Science, The University of Electro-Communications, Chofu, Tokyo 182-8585, Japan*

(Received 4 October 2010; published 28 February 2011)

When highly charged ions are incident on a surface, part of their potential energy is emitted as characteristic radiation. The energies and yields of these characteristic x rays have been measured for a series of elements at the Tokyo electron-beam ion trap. These data have been used to develop a simple model of the relaxation of the hollow atoms which are formed as the ion approaches the surface, as well as a set of semiempirical scaling laws, which allow for the ready calculation of the *K*-shell x-ray spectrum which would be produced by an arbitrary slow bare or hydrogenlike ion on a surface. These semiempirical scaling laws can be used to assess the merit of highly charged ion fluorescence x-ray generation in a wide range of applications.

DOI: 10.1103/PhysRevA.83.022901 PACS number(s): 34.35.+a, 32.30.Rj, 79.20.Rf

I. INTRODUCTION

A highly charged ion (HCI) is surrounded by an extremely strong electric field and has a large potential energy, equal to the energy required to liberate the electrons from the neutral atom to create the ion. This can be as much as several hundred keV for bare species of heavy elements.

When a highly charged ion is incident on a surface, it will begin to pull electrons from it at a significant distance due to the extremely strong fields which surround the ion. A portion of these electrons will be captured by the ion, typically into high-lying energy levels (with the principal quantum number of the capturing level going roughly as $n_c = q$, where q is the charge state of the ion) until it is neutralized, forming a so-called *hollow atom* whose inner shells remain almost entirely empty [1–4]. The excited electrons then begin to cascade down into lower energy orbitals, releasing energy either through Auger emission or, more relevantly for this application, fluorescence.

While this interaction has been studied extensively in terms of its effects on the surface (as the previously mentioned processes typically happen over time scales of femtoseconds, modifying the surface on the nanometer scale [5–7]), the x rays produced by fluorescence processes in this interaction have many properties which make them a potentially desirable x-ray source.

The most significant of these is their energies—since they result from x-ray transitions which are characteristic of the elements, they are produced only at specific energies with very small line widths. The exact energy at which they are generated also has good tunability, ranging from a few eV to over 100 keV across the range of natural elements.

While these x rays can in principle be produced by an electron falling into any shell, for most practical circumstances it would be *K*-shell fluorescence that is useful, because of its much higher energy. This means that the emission is much cleaner compared to that at lower energies, where other processes (such as bremsstrahlung from electrons pulled from the surface) also generate x rays, and significantly increases the range of applications where the source may be useful.

Taken together, these properties mean that HCI-surface interactions can be used to provide x rays with good energy specificity and tunability—properties which are typically associated with synchrotron radiation. While synchrotrons still have a significant advantage over the x rays produced through this method in terms of line widths and continuous tunability as opposed to the somewhat granular nature of tuning by changing the atomic number of the ions, the much lower cost and table-top nature of devices capable of producing highly charged ions of this type compared to a synchrotron means that this method has the potential to enable many of the applications which currently greatly depend on synchrotron sources at much smaller facilities.

Making specific predictions about the form of the *K*-shell x-ray fluorescence spectrum is very challenging, due to the nature of the collision and the multitude of possible stabilization pathways. However, it has been possible to effectively characterize these x-ray spectra through a few relatively simple scaling laws which describe the rate at which *K*-shell vacancies are filled through radiative transitions, and the energy of the resulting emission, which allows for the ready prediction of the x rays which would be produced by an arbitrary bare or hydrogenlike ion when incident on a surface.

These scaling laws taken together form the basis for predicting the x-ray spectrum due to *K*-shell filling of any bare or hydrogenlike ion impacting on a surface and are therefore useful for the planning or design of an x-ray source based on this principle.

II. METHODS

Experiments were carried out at the Tokyo EBIT [8] to characterize the fluorescence x-ray spectra which can be produced by this method. In this work, bare and hydrogenlike species of a selection of elements (ranging from argon to

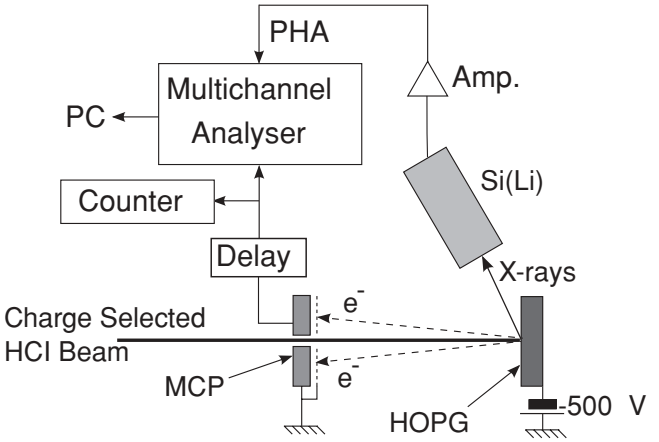

FIG. 1. Schematic illustration of experimental setup. Highly charged ions extracted from the Tokyo EBIT are incident on a graphite surface, and the resulting x-ray spectrum is measured.

iodine) were impacted onto a highly ordered pyrolytic graphite (HOPG) surface at low energies (equal to $q \times 3.5$ keV, where q is the charge state). The primary detector was a Canberra SL30165 Si(Li) x-ray detector, oriented at 60° to the target surface to detect x rays emitted by the impact of the HCIs. This detector had an active area of 30 mm^2, and was at 6 cm from the HCI impact site.

To provide a count of the number of HCI which impact on the surface, a multichannel plate (MCP) detector was used to detect and amplify the pulses of electrons produced by HCI impacts, and this total was used to calculate photon yields per ion in the measured data. The signal from the MCP was also used to gate the output of the x-ray detector to ensure that only events which were associated with HCI impacts were recorded. The experimental setup is schematically illustrated in Fig. 1.

The detector's energy response was calibrated using ^{55}Fe and ^{241}Am radioisotopes, which provide clean spectra at well-characterized energies, and a least-squares fit was performed to map the spectrometer channel numbers to energies. This was used to convert the x-ray channel counts into a function of energy, and the counts were divided by the channel width to give counts per keV.

To account for detector sensitivity and uncertainty in the measured solid angle in the experiment, the spectra were then normalized to previously observed data [9,10] to give a final value for the number of emitted x rays per keV per ion.

III. RESULTS

Spectra were measured for bare and hydrogenlike species of argon, manganese, yttrium, indium, and iodine. These elements have atomic numbers ranging from 18 to 53, and the resultant x-ray spectra range in energy from 3 to 40 keV. These spectra were analyzed to quantify the behavior of the emission, and corresponding scaling laws were developed to extend this description to other elements.

The spectra for the hydrogenlike and bare ions are plotted in Figs. 2 and 3, respectively. The low-energy range of each observed spectrum has not been plotted for clarity, leaving only the K-shell fluorescence which would be used in most

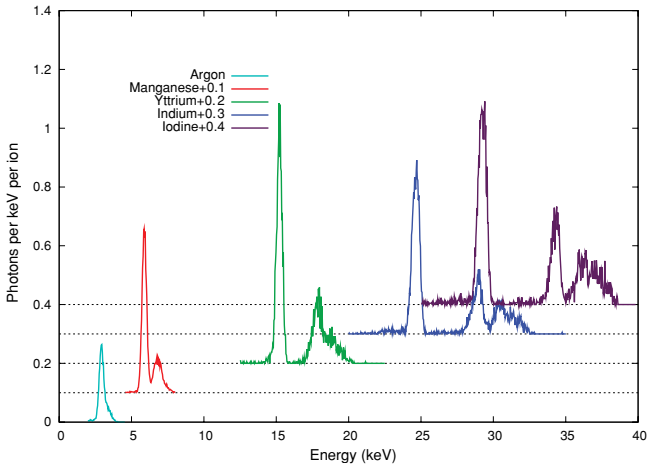

FIG. 2. (Color online) Fluorescence x-ray spectra from slow hydrogenlike ions incident on a graphite surface. The sharp x-ray features are produced when electrons transition from high-lying shells to the K shell. Other x rays at lower energies have been omitted for clarity. Spectra have been offset by the amounts indicated in the figure legend.

applications. In practice, this could be achieved through the use of a suitable x-ray filter.

As would be expected, each ion emits x rays corresponding to its $K\alpha$, $K\beta$, etc. transitions in several peaks, whose mean energy and separation increases with atomic number. These peaks are well approximated by a Gaussian, a profile which is primarily the result of the detector's response, as its rated full width at half maximum (FWHM) (∼2% at 5.9 keV) is on the order of the observed width. Some additional broadening would be expected because the exact energy levels involved in the transition would depend on the exact arrangement of other electrons in the system, but this fine detail is impossible

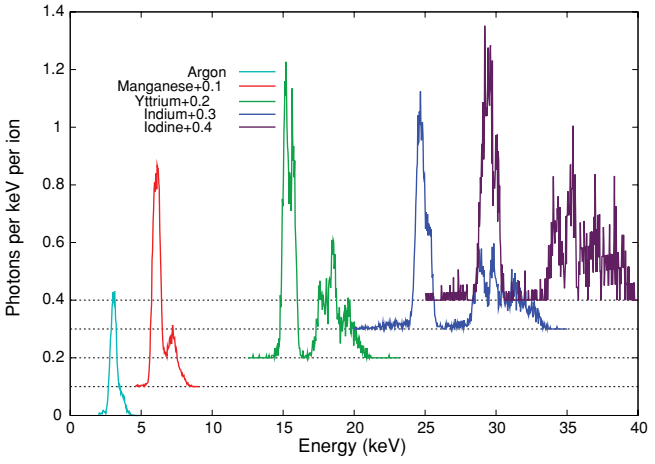

FIG. 3. (Color online) Fluorescence x-ray spectra from slow bare ions incident on a graphite surface. Once again the sharp x-ray features correspond to electron transitions from high-lying shells to the K shell, but with an increased yield per ion due to the additional K-shell vacancy in each ion. Low-energy x rays are again not plotted for clarity. Spectra have been offset by the amounts indicated in the figure legend.

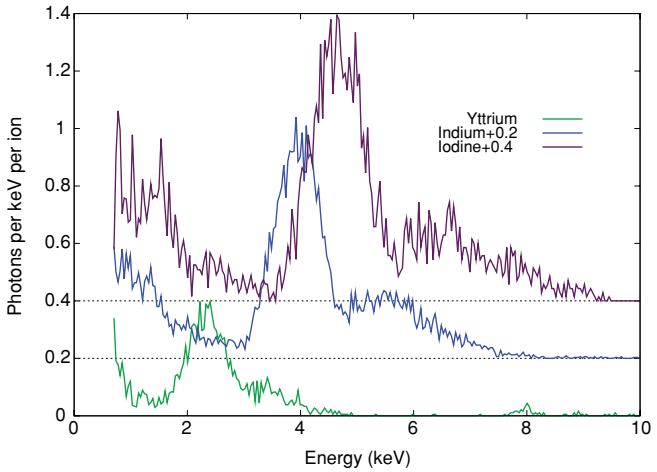

FIG. 4. (Color online) Low-energy portion of fluorescence x-ray spectra from slow hydrogenlike ions incident on a graphite surface. Here, comparatively broad peaks resulting from electrons falling into the L shell can be seen, together with an escalated background due to contributions from other processes such as bremsstrahlung. For all ions, no emission is observed between the L-shell peaks and the K-shell peaks as plotted in Fig. 2. Due to experimental limitations x rays below 750 eV were not measured, and as a result the spectra are truncated at this point, which prevents the plotting of the L-shell peaks for argon or manganese ions. Spectra have been offset by the amounts indicated in the figure legend.

to distinguish in this data, meaning that the peaks are simply treated as a single Gaussian for each transition.

These Gaussians can then be used to characterize the transitions, with their central value being taken as the energy of the transition, and with their total area being equal to the number of photons produced per ion by the transition, due to the corrections outlined previously.

Considering the bare spectra, the primary difference is the appearance of a second peak for each transition, at a slightly higher energy. This is the result of the filling of the extra K-shell vacancy, which emits at a slightly higher energy due to the lack of the screening which is present in the hydrogenlike case. Despite the increased yield per ion, the total number of ions produced (and thus the quality of statistics in these plots) is significantly reduced, particularly for high-Z ions, due to the added difficulty of producing completely bare species.

An example of the low-energy portion of the emission from hydrogenlike ions is illustrated in Fig. 4. Once again a series of peaks is apparent for each element, in this case corresponding to electrons falling into the L shell of the ions, along with an elevated background at energies below the peaks, believed to be the result of other processes such as bremsstrahlung. The energy specificity of these transitions can be seen to be much poorer than those produced from K-shell transitions, with individual peaks having widths of 10% or more. This combination of factors makes L-shell emission a much less desirable source of x rays. Fortunately, due to the large energy range between these x rays and those produced by K-shell emission (which can be seen to differ by roughly a factor of four, corresponding to the ratio of the K- and L-shell binding energies) where no emission occurs, these x rays can be readily removed by a suitable metal filter without significantly reducing the fluence of the useful K-shell emission. Similar results are observed for the bare ion emission (data not shown).

IV. ANALYSIS

To parametrize the spectrum for each ion, Gaussians were fitted to each of the resolvable peaks (two for argon, three for the other ions), corresponding to the $K\alpha$, $K\beta$, and $K \geqslant \gamma$ transitions. These Gaussians were characterized by their area (the per ion x-ray yield for the transitions), their mean energy value, and their standard deviation (proportional to the measured width of the transition). The $K\gamma$ and higher transitions have been grouped as a single peak because they are not well resolved in this data, meaning they cannot be meaningfully fit as distinct peaks. However, it can be seen that these aggregate peaks remain broadly Gaussian in form, and can be fit reasonably well as a single peak, albeit with greater width than the clearly resolved $K\alpha$ and $K\beta$ peaks.

Attempting to fit to all six peaks for the bare ion cases was found to be unfeasible, as parameters describing adjacent peaks were highly correlated, leading to very poorly conditioned fits. To account for this, a spectrum which corresponds to only the unscreened transitions was generated by subtracting the hydrogenlike spectrum from the bare ion spectrum, based on the assumption that the additional K-shell vacancy is simply additive and entirely independent of the hydrogenlike emission. The resulting spectra are shown in Fig. 5. It can be seen that its form is very similar to that of the hydrogenlike data, which suggests that this was a reasonable assumption. The level of noise is necessarily higher, as a result of taking the difference between the two spectra, but the overall form remains clear.

A. Transition energy

For the energy scaling, transition energies were predicted based on the energy levels of a hydrogenlike ion, with charge Z for the case where the ion was bare before arriving at the surface, and $Z - 1$ for the case where the ion was initially

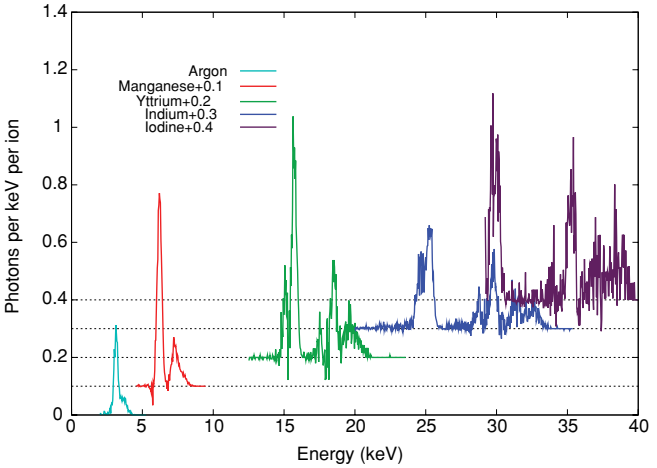

FIG. 5. (Color online) Fluorescence x rays resulting from unscreened transitions into the K shell in bare ions, produced by taking the difference between the total bare ion spectra and the hydrogenlike spectra. Spectra have been offset by the amounts indicated in the figure legend.

hydrogenlike, to account for the screening provided by the initial K-shell electron.

This neglects any potential screening effects from the other electrons in high-lying energy levels, but this is expected to be a small effect. There are two reasons for this—firstly, since these electrons are in high-lying energy states, they are distant from the nucleus and are unlikely to strongly affect the low-lying energy levels; secondly, the transition rate for radiative transitions scales strongly with the energy of the transition (as $\sim E^3$), meaning that the largest transitions typically occur relatively rapidly. Thus, a transition into the K shell will occur very rapidly after an electron falls into an energy level from which it can relax radiatively, typically before additional electrons cascade downward through the Auger effect. As a result, it would be expected that the electron which fills the K-shell vacancy would be one of the first to reach the lower energy levels where radiative states make up a larger proportion of the total number of states. This means that these lower energy levels would still be relatively sparsely populated when the transition occurs, with a correspondingly weak screening effect.

As a result, it would be expected that the electron which fills the K-shell vacancy would be one of the earliest electrons to reach low-energy levels, meaning these levels remain sparsely populated, leading to relatively weak screening.

To describe these pseudohydrogenic energy levels, the Dirac model of the hydrogen atom is used. The Dirac model is chosen over simpler models because it includes relativistic corrections which are a significant factor for high-Z ions. It describes the energy levels of a hydrogenlike atom as

$$E = -\frac{\mu e^4 Z_{\text{eff}}^2}{(4\pi\epsilon_0)^2 2\hbar^2 n^2}\left[1 + \frac{Z_{\text{eff}}^2\alpha^2}{n^2}\left(\frac{n}{j+1/2} - \frac{3}{4}\right)\right], \qquad (1)$$

where all symbols have their usual meaning [11]. Z_{eff} is the *effective* atomic number—for ions which are initially hydrogenlike, this is taken as the atomic number of the element minus one. Using this equation, the binding energy of each level can be readily calculated for any element, which in turn can be used to predict the energy of the transitions by taking their differences.

Since the three peaks correspond to the $K\alpha$, $K\beta$, and predominately $K\gamma$ transitions, their initial and final n values are uniquely specified, as well as the angular momentum (j) value of the ground state. However, for each upper state there exists a series of possible j values (from $\frac{1}{2}$ to $n - \frac{1}{2}$), which cannot be resolved in this data.

As a result, a choice has to be made about which j value to assign to the upper state for these transitions. While dipole-forbidden transitions do become more common for high-Z ions, the rate of dipole-allowed transitions remains much greater than these forbidden transitions, so only dipole-allowed states of $j = 1/2$ and $j = 3/2$ are considered for the upper states. Since these transitions cannot be clearly resolved, the predicted energy was set as the weighted average of the two energy levels according to the number of electrons which could participate in each type of transition.

A comparison of the observed and predicted energies is plotted for hydrogenlike ions and the unscreened transitions in bare ions (in Figs. 6 and 7).

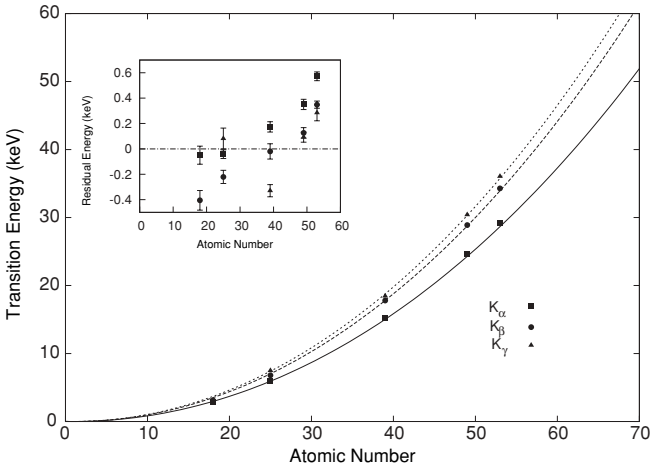

FIG. 6. Dependence of energy of x-ray fluorescence with atomic number for hydrogenlike ions. Plotted are fitted transition energies from observed spectra (points), as well as energies predicted by considering Dirac energy levels for the ion as discussed in the text (curves). Error bars on transition energy fits are obscured by the symbols. (Inset) Residuals of observed values compared to fits.

The agreement between the curves is good, with disagreements typically on the order of a few hundred electron volts between the predicted and observed values at all energies. The main source of this disagreement is the effect of the other electrons, which are neglected in the previous calculation of the energy levels. This can be clearly seen in the residuals plot for bare ions (Fig. 7, inset), where the predictions typically overestimate the energy levels by a small amount, which would be the expected effect of the other electrons in the system. The magnitude of this overestimation reduces with increasing atomic number, suggesting that the effect of this screening is less significant in ions of higher atomic number.

While the overall quality of agreement between predictions and observation for the hydrogenlike ions is similar, the difference between the predicted and observed values is more complex. At low atomic numbers, the predictions systematically overestimate transition energies, as in the bare case.

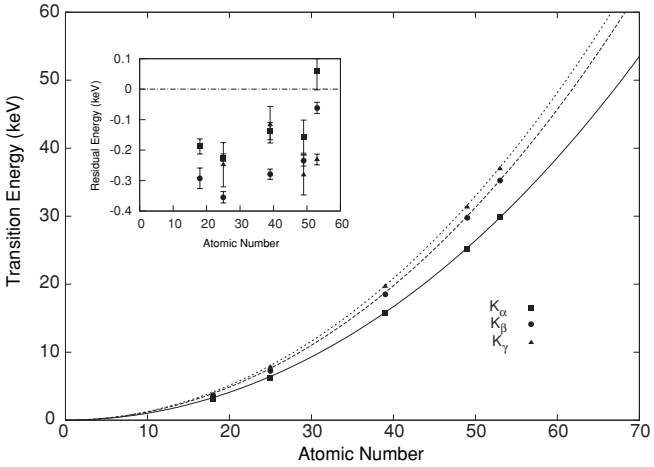

FIG. 7. Dependence of energy of x-ray fluorescence with atomic number for unscreened transitions in bare ions. Data prepared and presented as in Fig. 6.

However, at higher energies the observed energies become higher than the predicted energies, seemingly in contrast with the effects of screening. One explanation for this is to note that hydrogenlike ions are represented in this model simply as a bare ion of atomic number 1 lower, and that this approximation breaks down in the case of high atomic numbers.

While these various screening effects can potentially be taken into account, it would involve a substantial increase in the complexity of the model used to calculate the energy levels, both in terms of working out the possible electron distributions, as well as the resulting energy levels. With this in mind, it can be seen that this model strikes a good balance, allowing for a very simple calculation to be carried out to obtain the energies of any transition at good accuracy (better than ∼3% over most elements), and the relatively constant magnitude of the discrepancy between the observed and predicted energies for the unscreened transitions indicates that the effects of screening by outer-shell electrons is not a significant factor in determining the K-shell fluorescence energy, being limited to differences of a few hundred eV for all ions.

B. Production rate—theoretical

The photon production rates are a more complex property—while their general qualitative behavior (a gradual increase in photon yield, reaching 1 photon/ion at high atomic numbers as would be expected from the filling of the single K-shell vacancy) is easy to understand, a more robust quantification and an understanding of the underlying processes is desirable.

Since it is known that radiative processes compete with Auger transitions to stabilize hollow atoms, the production rates were investigated in terms of these processes. A full, robust model of the relaxation processes for hollow atoms across all atomic numbers is an extremely challenging task, far beyond the scope of this work. However, a simple model is developed here, incorporating the key aspects of the physics underlying this system. It is found that, despite neglecting many of the complex behaviors of the system, this model is capable of well reproducing the behavior of the production rates as a function of atomic number.

The conceptual model of this system is well established in the literature [2,3,12,13], and can be summarized as follows: Firstly, it is assumed that an ion approaching a surface very rapidly captures electrons from the surface, such that it quickly becomes neutral, with the captured electrons arriving in very high-lying energy levels before any relaxation occurs. These electrons then begin to cascade down, through a combination of Auger and fluorescence processes, with the former dominating very strongly for all but the most inner-shell transitions. Since the approach of the ion will have removed many more electrons from the surface than are needed for the initial neutralization, it is also assumed that any electrons ejected through the Auger process are replaced immediately by capture into the same high-lying energy levels as the initial electron population.

Eventually, an electron will make a transition to the $n = 1$ shell, through the emission of either an Auger electron or a fluorescence photon. By simulating this process for a very large number of electrons and recording the nature of the process responsible for the filling of the $n = 1$ vacancy, predictions can be made about the yield of photons for a given HCI.

While the relaxation process as described previously is conceptually very straightforward, the technical details remain challenging to implement. Even the calculation of the basic rates of individual Auger and fluorescence processes for the various electron distribution is unfeasible, due to the myriad possible configurations. Taking iodine as an example, if 53 electrons are distributed in energy levels up to $n = 53$, there are on the order of $\sim 10^{200}$ possible electron distributions, each of which will have a distinct set of transitions and associated rates. This great number of states also places a very high demand on the number of HCI impacts which must be simulated to provide good statistics. To complete these calculations in a feasible time frame, further simplifications must be made.

For example, rather than calculating all of the rates for the individual transitions from first principles, rates were obtained from published data sets (in particular, the Evaluated Atomic Data Library (EADL) [14–16]). While these data sets only deal with the case of a single vacancy in an otherwise unperturbed ion, they do provide a reasonable starting point for the relative rates of different transitions.

A more significant limitation of the EADL data sets is the limited number of n orbitals which are represented—even the heaviest elements only have $n = 5$ and lower shells occupied. Since in this scenario electron capture typically occurs into much higher orbitals, this is obviously insufficient.

To address this, a scaling law was developed to extrapolate these data sets to include vacancies in higher shells. An empirical scaling law was derived which was found to agree well with the Auger scaling rates in the EADL and the work of McGuire [15,16]. Specifically, the rate of an arbitrary Auger transition A_{xyz} is characterized as

$$A_{xyz} \propto \gamma^{-x} e^{-\alpha(y-x)} e^{-\beta(z-y)},$$

where x, y, and z are the principal quantum numbers of the vacancy, the lower transitioning electron and the upper transitioning electron, respectively; α, β, and γ are fitting constants. These constants, as well as the proportionality constant, were found by fitting this expression to the published Auger rates for heavy elements, which had the greatest representation of high-lying orbitals.

While α, β, and γ are reasonably independent of Z, the proportionality constant (and thus the absolute rate of all of the Auger transitions) scales with Z. This scaling law was fitted to through the use of the K-shell Auger data of McGuire, and was found to be well described by a relation of the form $A_{KLL} = A \ln(Z) - C$, where A and C are once again fitting constants. These two scaling laws were then used to extend the published rates to encompass all of those used in this work.

It should be noted that these scaling laws are largely approximate, as there are many complex dependencies of Auger rates on atomic number and the exact electron configuration present in the ion. However, these are a useful basis for this model as they are much more readily calculable than through a full theoretical treatment.

A further simplifying step was to neglect radiative for all transitions where the electron does not make a transition into an angular momentum state of $j = \frac{1}{2}$. While this may appear to be a very drastic omission, it can be seen from the

EADL that the rate of radiative transitions from such states is typically on the order of 1% or less than that of the competing Auger transitions, even in the lowest shells—and this falls to one part in a million or more for higher orbitals. While this approximation does begin to break down somewhat for low-lying shells in the heaviest elements considered in this study (with the possibility of radiative filling of the $L_{2,3}$ states in iodine having rates on the order of a few % for some electron configurations), this inaccuracy is offset by the greatly reduced number of possible transitions and properties which must be tracked, which significantly simplifies the implementation of the simulation.

The previously mentioned decisions alone do not dramatically influence the time taken to process these simulations, as there remains a tremendous number of possible configurations of electron states, meaning complete simulations remain very time-consuming. However, by neglecting the radiative transitions from most states, it is possible to greatly simplify the number of states which must be considered.

Specifically, it is possible to merge all of the states in a given shell into a single superstate, described only by its principal quantum number n, by summing over the rates of all of the individual Auger transitions involving different angular momentum states for that principal quantum number. This reduces the number of possible configurations and rates which must be considered by several orders of magnitude, greatly simplifying the implementation of this system.

The average behavior of this approximation (when used with a Monte Carlo approach) over many runs appears to be reasonable for Auger transitions, but care must be taken for radiative transitions. As noted previously, selection rules are much more important in this case, meaning in many cases the dominant factor in whether a radiative transition will occur is not its rate relative to the competing Auger transitions, but whether or not it fell into a suitable angular momentum state, with allowed transitions almost certainly happening, and forbidden transitions effectively never occurring.

To represent this effect, while each electron's state was primarily recorded just in terms of their n value, an additional flag was associated with each electron, relating to whether it was in a "radiative-ready" state or not (that is, capable of reaching a $j = \frac{1}{2}$ state through a dipole-allowed radiative transition).

This flag was determined in a purely probabilistic fashion—when an electron entered a new n level (either during its initial capture, or after falling due to an Auger transition) a random number in the range $[0,1]$ is generated. If this was less than the ratio of the number of unoccupied radiative-ready states to the total number of states in the energy level, the electron was tagged as being radiative ready and was considered as a candidate for both radiative and Auger relaxation in future time steps. If not, then it was only considered for Auger transitions.

This simple model provides a much more computationally tractable problem, allowing for the simulation of hollow atom cascades for a range of elements in tractable time scales. However, while the previously mentioned model covers the dynamics of the system, the initial condition of the electron distribution must also be determined.

As noted earlier, models of ion-surface interactions suggest that electrons would be captured into an energy level with $n_{\text{initial}} = Z$ for bare ions [2]. However, implementing this behavior is challenging, for two reasons.

Firstly, the extrapolations of Auger and radiative rates are built from data which only covers shells up to $n = 5$. Extending this to states whose principal quantum numbers are 10–20 times greater runs the risk of substantial systematic errors.

Secondly, the number of transitions which occur before the K-shell filling transition depends very strongly on the initial state the electrons are captured into. There is a very large amount of "churn" in the highest energy levels, with many rapid, small transitions taking place as electrons move a few shells lower before being ejected, which does not significantly contribute to the overall relaxation toward filling the K shell [3]. This problem is greatly exacerbated with increasing n_{initial}, with the average time taken for a single relaxation simulation almost doubling if n_{initial} is increased by 1.

To mitigate these problems, all simulations were started with all of the electrons distributed in a single shell, which was chosen as $n_{\text{initial}} = 10$. While this is small compared to the energy levels which electrons are typically captured into at long ranges from the surface through the over-the-barrier process (with captured states roughly given by $n \approx Z$), a majority of hollow atoms formed outside the surface will not relax fully before reaching the surface, and a number of weakly bound electrons will be "peeled off" by impact with the surface [17]. Once the ion is within the surface, there exists the possibility for the filling of energy levels by charge transfer from overlapping levels in the target material through "side-feeding" processes [18,19].

Side feeding can lead to capture into much more tightly bound energy levels than the over-the-barrier model, even into L-shell orbitals in light elements. However, because of the combination of the high atomic number of the ions considered in this work and the light nature of the target, the electrons which are available from the bulk material are still weakly bound compared to many of the tightly bound levels in the ions used in this work. As a result, filling of the innermost shells remains unlikely, with the greatest overlap between states happening for higher energy levels, suggesting that creating initial populations in an intermediate energy level is a reasonable approach.

This was supported by empirical observations of the quality of agreement between the observed and predicted photon yields, with $n_{\text{initial}} = 10$ providing good qualitative agreement in practical time frames. There is a degree of disagreement with respect to higher transitions, but this is unsurprising, since higher starting shells reduce the probability of Auger events filling low-lying shells and correspondingly increase the chance that electrons in high shells will arrive in a state where dipole-allowed radiative relaxation is possible. However, the dependence of these higher transitions on n_{initial} is relatively weak above $n_{\text{initial}} = 10$, meaning that substantially improving on the agreement simply by increasing n_{initial} was not a viable approach.

A simple Monte Carlo code was developed which implemented the previously mentioned model of the relaxation process, simulating an electron population where they were all initially in the $n = 10$ shell and tracking its relaxation. In this model, rates for all possible transitions are calculated for the configuration at each step, and one is chosen randomly

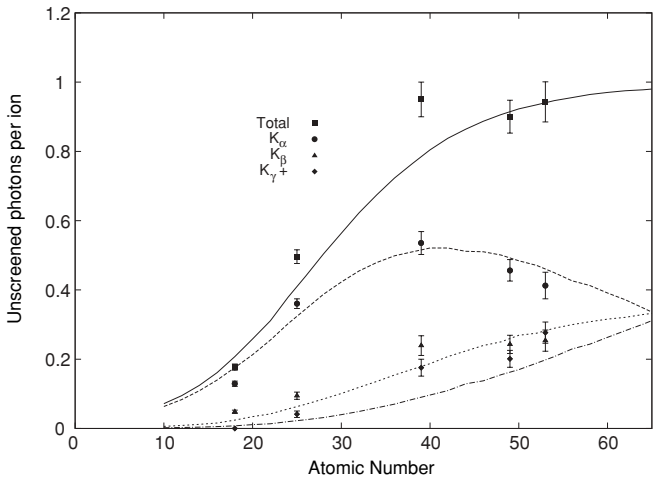

FIG. 8. Comparison of the theoretical Monte Carlo model to observed production rates for unscreened transitions in bare ions. Here the total production rate, and rates for $K\alpha$, $K\beta$, and $K\gamma$ and higher transitions are plotted for both the observed values (points) and the theoretically predicted dependence (lines). The overall behavior of the system is well represented, with reasonable agreement across all Z values.

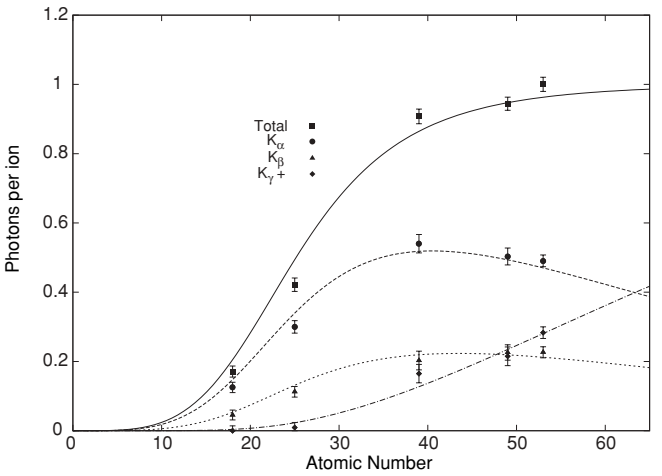

FIG. 9. Photon yield as a function of atomic number for hydrogenlike ions, considering both total production and rates for individual transitions. Points are rates which are calculated by integrating under curves from experimental results, while lines are empirically fitted production rates as described in the text.

(weighted according to their rates). The electron configuration is updated according to the chosen transition (which, in all cases, involves one electron falling to a lower state, and the emission of either an Auger electron or fluorescence photon). If an electron is ejected by the Auger process, it is immediately replaced by a new one in the $n = 10$ state into which the electrons are initially distributed. This process is repeated until a transition into the K shell occurs, at which point the simulation halts. The fluorescence photons emitted for each relaxation are recorded, allowing a prediction of the photon yields to be built up over many repeated iterations of the code.

This code was run 1 million times for ions with atomic numbers ranging from 10 to 70, and the results are plotted, along with the corresponding measured rates for the unscreened transition in bare ions (in Fig. 8). It can be seen that this simple model quite effectively reproduces the qualitative behavior of the system, both in terms of the total yield which gradually increases toward 1 photon per ion at high Z, and the distribution of photons between individual transitions, with the $K\alpha$ transition initially dominating, but turning over and beginning to lose significance due to increased competition from other transitions at high atomic numbers. The quantitative agreement is also reasonably good, particularly for the $K\alpha$ transition, although the $K\beta$ and $K \geqslant \gamma$ transitions are less good, for reasons outlined previously.

As the model does not include the effects of screening, the production yields predicted the model for transitions in hydrogenlike ions are almost identical to those plotted in Fig. 8, and so are not plotted. The qualitative agreement, however, remains quite good, as the overall behavior does not significantly change between the unscreened and hydrogenlike transitions (as can be seen below in Figs. 9 and 10).

In both cases there is some quantitative disagreement, but it is very encouraging that this model, designed to encapsulate the essential physics in as straightforward a way as possible, is able to reasonably describe the results of such a complex physical processes. This provides a useful starting point for understanding this process, as well as a benchmark for comparison with more complex models.

C. Production rate—empirical

Expanding the theoretical model sufficiently to encompass more of the underlying physics and improve the quantitative agreement is, as noted previously, a very complex task, and beyond the scope of this work. However, it is possible to develop an empirical method to describe this process, based on the understanding derived from the previously mentioned

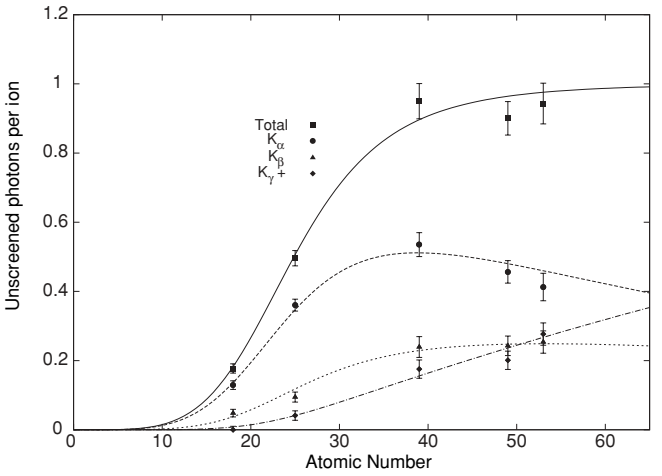

FIG. 10. Photon yield as a function of atomic number for unscreened K-shell transitions in bare ions, considering both total production and rates for individual transitions. Points are rates which are calculated by integrating under curves from experimental results, while lines are empirically fitted production rates as described in the text.

model. This not only offers a more quantitatively accurate description, but also has the advantage of being very compact and easy to implement, making it easily usable as a source of spectra to model applications involving this approach to x-ray generation.

Based on assumptions similar to those outlined in the previously mentioned theoretical model, the selection of the K-shell filling process is described in terms of competition between the rates of various processes, that is,

$$Y_\alpha = \frac{R_\alpha}{R_\alpha + R_\beta + R_{\geqslant\gamma} + R_{\text{Auger}}}, \tag{2}$$

where Y_α is the yield of the $K\alpha$ transition in photons/ion, and R is the rate of the transition denoted by its subscript. Similar equations can be obtained for other transitions by replacing the numerator in (2) with the appropriate rate. The rates of the transitions can be expressed as an $R = A(Z_{\text{eff}})^m$, where m denotes how strongly the process scales with atomic number, and A is a rate constant.

However, it is not possible to fit Eq. (2) meaningfully in this form. It can be seen that it is poorly conditioned in both A and m, so one rate must be fixed as a constant value and the others expressed as relative rates to correct for this. Since this work is primarily concerned with the behavior of the radiative transitions, the obvious choice is to fix the Auger rate equal to 1. This then means that the relative rates are expressed as, for example, $R_\alpha^{\text{Rel}} = (A_\alpha/A_{\text{Auger}})(Z_{\text{eff}})^{(m_\alpha - m_{\text{Auger}})}$ for the $K\alpha$ rate.

One benefit of choosing the Auger transition as the fixed rate is that, because it depends very weakly on atomic number, $m_{\text{Auger}} \approx 0$, meaning the scaling coefficients which are obtained from the fit can be taken as being the absolute scaling of the process. To improve the quality of the fit on the rate constant, the rates are re-expressed as $R_\alpha^{\text{Rel}} = (Z_{\text{eff}}/B_\alpha)^{m_\alpha}$. Here, the ratio of rate constants has been replaced by dividing the effective atomic number by a new constant, B, which can be considered as the atomic number at which the probability of that radiative transition filling the K shell is equal to the probability of it being filled by an Auger transition. This removes the otherwise very strong dependence of the rate constant parameter on the scaling parameter. With these changes, Eq. (2) can be expressed as

$$Y_\alpha = \frac{\left(\frac{Z_{\text{eff}}}{B_\alpha}\right)^{m_\alpha}}{\left(\frac{Z_{\text{eff}}}{B_\alpha}\right)^{m_\alpha} + \left(\frac{Z_{\text{eff}}}{B_\beta}\right)^{m_\beta} + \left(\frac{Z_{\text{eff}}}{B_{\geqslant\gamma}}\right)^{m_{\geqslant\gamma}} + 1}, \tag{3}$$

and similarly for other transitions.

Equation (3) was fitted to the observed values for the transition rates in both the hydrogenlike and unscreened cases. The resulting curves are plotted along with the observed values in Figs. 9 and 10, respectively. The agreement here is good, once again reflecting the qualitative behavior of the system, but now also providing superior qualitative agreement, especially for higher transitions. The values obtained for the parameters describing this system are shown in Tables I and II.

From these tables, it can be seen that the scaling rate for the $K\alpha$ transition agrees very well with the theoretically predicted scaling rate of fluorescence transitions, which scale as Z^4 [20]. By contrast, the $K\beta$ and $K \geqslant \gamma$ transitions show stronger scalings with atomic number; this is in agreement with discussions earlier, which noted that the shell into which the electrons are initially captured had an additional influence on the probability of seeing transitions from higher shells. The B values also generally support these observations, with radiative transitions from higher shells becoming significant compared to Auger transitions at gradually increasing atomic numbers.

TABLE I. Parameters describing hydrogenlike fluorescence x-ray yield, fitted as described in the text.

	B	m
$K\alpha$	28.7 ± 0.6	3.9 ± 0.2
$K\beta$	35 ± 1	4.3 ± 0.2
$K\gamma$	39 ± 1	7.0 ± 0.4

Comparing the hydrogenlike and unscreened transitions, there does appear to be a slight difference, with the unscreened transitions having a faster onset and scaling more rapidly, with generally lower B values and greater scaling coefficients. However, the two sets of curves are still very similar, overlapping within the error bars at most points, indicating that despite these small differences the overall behaviors of the screened and unscreened K-shell transitions are very similar.

Once again, it can be seen that an extremely simple analytic fit is able to describe the behavior of this system to a surprisingly high degree of accuracy, based on a relatively simple model. This in principle allows for the rapid calculation of the x-ray yield of each transition for any element with good accuracy, although care may need to be taken with extrapolating to very heavy elements, as extrapolating scalings with such strong dependence on Z may cause inaccuracies.

D. Transition line width

The final factor to describe the transitions—the line width—is difficult to accurately characterize, because as noted earlier the observed line width results in large part from the response of the detector system, making the true width impossible to determine directly from these data. However, it is also unreasonable to assume that the detector response is entirely responsible for the width of this peak, as in other, high-resolution measurements of x rays produced by HCIs incident on surfaces (such as [2]) it has been seen the screening from electrons in nearby shells causes a broadening in the line width of the fluorescence from HCI impacts.

The apparent single peak of the $K\alpha$ transition in hydrogenlike argon has been shown to actually be made up of a series of peaks, with an energy spread of roughly 3% about the central value [2]. This is in good agreement with our observations, which suggest a width of 4% for the same transition, in line

TABLE II. Parameters describing unscreened fluorescence x-ray yield from bare ions, fitted as described in the text.

	B	m
$K\alpha$	27.1 ± 0.8	4.4 ± 0.3
$K\beta$	33.3 ± 1.3	5.0 ± 0.4
$K\gamma$	37 ± 1.0	6.5 ± 0.4

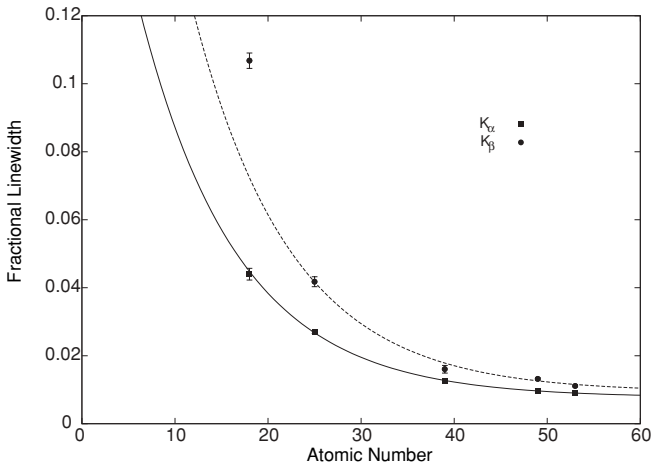

FIG. 11. Dependence of fractional line width σ/E as a function of atomic number. Points are measured values from observed spectra; lines are an empirical fit to the data. The $K\beta$ point for argon has been excluded from the fit, due to the lack of differentiation between it and the neighboring $K\gamma$ peak.

with the convolution of this peak spread with our detector's resolution.

Considering the shape of the peaks in Figs. 2 and 5, it can be seen that the widths of these peaks do not increase dramatically with increasing energy, suggesting that the fractional energy spread (that is, σ/E, where σ is the standard deviation of the fitted Gaussian and E is its central energy) is not constant. To illustrate this, the fractional energy spreads are plotted in Fig. 11 for the $K\alpha$ and $K\beta$ transitions as a function of atomic number for hydrogenlike transitions. The behavior of line widths for bare ions is omitted as it does not differ significantly from these results.

This clearly shows a reduction in the fractional width of peaks with increasing energy. This can be explained by noting that the rate of radiative transitions increases dramatically with increasing atomic number, meaning that there is less time for additional electrons to fall into low shells and partially screen these transitions, causing a reduction in the possible energy spread.

An empirical fit has been made to the data and also plotted in Fig. 11. The $K\beta$ transition from argon has been omitted from this fit, as its width is exaggerated due to the inability to distinguish the $K \geqslant \gamma$ transitions from it in these data. The fit was of the form,

$$\frac{\sigma}{E}(Z) = Ae^{-\frac{Z}{B}} + C, \tag{4}$$

where A, B, and C are fitting constants, which are tabulated in Table III.

TABLE III. Parameters describing the line widths of transitions as a function of atomic number, fitted as described in the text.

	A	B	C
$K\alpha$	0.21 ± 0.02	10.5 ± 0.4	0.008 ± 0.001
$K\beta$	0.34 ± 0.3	10.5 ± 4	0.009 ± 0.03

It can be seen that C, which can be interpreted as the line width in the high Z limit, approaches values which agree very well with the response of the detector (which corresponds to a σ/E of $\sim$0.85% [21], verified by examination of the isotope calibration spectra), which suggests the effects of other electron screening is very small for K-shell transitions in the high-Z limit. Considering the case for lighter ions, the rate at which the fractional line width reduces appears to be identical between the $K\alpha$ and $K\beta$ transitions, with only the magnitude of the screening changing between the two types of transitions. Thus, a good estimate of the true line width for a given transition, taking into account the screening by other electrons, can be obtained by omitting C from Eq. (4) and using the appropriate values in Table III.

The analysis of the $K \geqslant \gamma$ and higher transitions is not so straightforward, however, as this peak is actually made up of varying contributions from multiple transitions with different energies, meaning the measured width does not follow the same relationship as the other transitions.

As an alternative to this, a single fixed width can be applied to the $K \geqslant \gamma$ transitions, which reflects the spread of transitions which contribute to this peak. Applying Eq. (1), it can be calculated that the maximum separation from the $K \geqslant \gamma$ transition to a transition from any higher shell is 7%. If the $K \geqslant \gamma$ energy is then taken as the central energy of this entire family of transitions, then a line width of half of this seems to be a reasonable estimate, that is, a σ/E value of 3.5%. While this is not likely to precisely reflect the distribution of these transitions, it is unlikely to dramatically change the appearance of the spectrum, and moreover any errors will be on the order of a few % shift in an often small fraction of the total spectrum, which would be negligible for most applications.

Taken together, Eqs. (1), (3), and (4), together with the data presented in Tables I–III offer a set of rules based on relatively straightforward physical principles which allowing for the ready calculation of the x-ray spectra which would be expected from the impact of an arbitrary bare or hydrogenlike HCI on a HOPG surface.

V. DISCUSSION

The relaxation of hollow atoms is a very complex process and any complete description of its behavior is very challenging. Despite this, it has been shown that a model can be developed from relatively simple physical principles which describes the end points discussed in this work very well. Additionally, from this understanding, simple scaling laws can be developed which give an accurate prediction of all of the characteristics of the x-ray spectra produced by this process (with all parameters characterized to accuracies of better than 5%, often significantly so).

This allows for the easy evaluation of the potential efficacy of x-ray generators of this type for a variety of applications, without the need for extremely detailed calculations. The most obvious property to take advantage of in these spectra is their energy specificity, which is potentially valuable for applications which involve targeting absorption edges in specific elements, such as two-energy CT imaging [22] or contrast enhanced radiotherapy [23], or which seek to study diffraction patterns.

Additionally, it is possible to guide HCIs through tapered capillaries [24], allowing for micrometer-spot sizes to be achieved. Since the range over which the HCIs emit energy when incident on a surface is small compared to this, this means that a very well-defined x-ray point source can be achieved, which has potential applications in, for example, phase contrast imaging [25] or as an x-ray microbeam [26].

Overall, these spectra offer an intermediate point between broad-band sources and synchrotron light delivered through a monochromator, in terms of energy specificity, tunability, and spot size at a relatively low cost.

VI. CONCLUSIONS

The x-ray spectra produced by the impact of highly charged ions on HOPG surfaces were analyzed, based on data obtained at the Tokyo EBIT. A simple physical model was developed which predicted, from first principles, the general behavior of the system, and which provided the basis for a set of semiempirical scaling laws which served to describe the behavior of the system with good quantitative agreement.

Although the scaling laws described in this work were derived by considering elements with atomic numbers ranging from 18 to 53, the rules which were derived are not fundamentally limited to this range, and so can be extrapolated to elements outside this range—although care should naturally be used when extending data to significantly higher atomic numbers.

While this work can be refined further—by expanding the underlying data set, or by refining the models underlying these scaling laws—the rules presented here still offer a reasonably accurate and very quick method of predicting the x-ray spectra which would be produced from such a HCI impact, allowing for the rapid evaluation of the usefulness of this type of source for applications without extensive calculations.

[1] H. Ryufuku, K. Sasaki, and T. Watanabe, Phys. Rev. A **21**, 745 (1980).

[2] J. P. Briand, L. De Billy, P. Charles, S. Essabaa, and P. Briand, Phys. Rev. Lett. **65**, 159 (1990).

[3] H. Winter and F. Aumayr, J. Phys. B **32**, R39 (1999).

[4] N. Vaeck, J. E. Hansen, P. Palmeri, P. Quinet, N. Zitane, M. Godefroid, S. Fritzsche, and N. Kylstra, Phys. Scr. T **95**, 68 (2001).

[5] K. Mochiji, S. Yamamoto, H. Shimizu, S. Ohtani, T. Seguchi, and N. Kobayashi, J. Appl. Phys. **82**, 6037 (1997).

[6] I. C. Gebeshuber, S. Cernusca, F. Aumayr, and H. P. Winter, Int. J. Mass Spectrom. **229**, 27 (2003).

[7] Y. Baba, K. Nagata, S. Takahashi, N. Nakamura, N. Yoshiyasu, M. Sakurai, C. Yamada, S. Ohtani, and M. Tona, Surf. Sci. **599**, 248 (2005).

[8] F. J. Currell *et al.*, J. Phys. Soc. Jpn. **65**, 649 (1996).

[9] H. Watanabe, S. Takahashi, M. Tona, N. Yoshiyasu, N. Nakamura, M. Sakurai, C. Yamada, and S. Ohtani, Phys. Rev. A **74**, 042901 (2006).

[10] J. Sun, H. Watanabe, M. Tona, T. Watanabe, N. Nakamura, C. Yamada, and S. Ohtani, Phys. Rev. A **77**, 032901 (2008).

[11] R. Eisberg and R. Resnick, *Quantum Physics of Atoms, Molecules, Solids, Nuclei, and Particles* (John Wiley & Sons, New York, 1985).

[12] J. Burgdörfer, P. Lerner, and Fred Meyer, Phys. Rev. A **44**, 5674 (1991).

[13] H. P. Winter, F. Aumayr, Y. Yamazaki, N. Stolterfoht, and U. Thumm, *Physics of Multiply and Highly Charged Ions*, 1st ed., Vol. 2 (Kluewr Academic Publishers, Dordrecht, 2003).

[14] S. T. Perkins, D. E. Cullen, M. H. Chen, J. Rathkopf, J. Scofield, and J. H. Hubbell, Technical Report, UCRL-50400, Vol. 30, Lawrence Livermore National Laboratory, CA, 1991.

[15] E. J. McGuire, Phys. Rev. A **2**, 273 (1970).

[16] E. J. McGuire, Phys. Rev. A **3**, 1801 (1971).

[17] J. Burgdörfer, C. Reinhold, and F. Meyer, Nucl. Instrum. Methods in Physics Research Section B **98**, 415 (1995).

[18] L. Folkerts and R. Morgenstern, Europhys. Lett. **13**, 377 (1990).

[19] U. Thumm, *The Physics of Multiply and Highly Charged Ions* (Kluwer Academic, New York, 2003).

[20] J. D. Gillaspy, J. Phys. B **34**, R93 (2001).

[21] *Canberra SL30165 Detector Specifications and Performance Data* (Canberra, Meriden, 2005).

[22] F. A. Dilmanian *et al.*, Physics in Medicine and Biology **42**, 371 (1997).

[23] S. J. McMahon, M. H. Mendenhall, S. Jain, and F. Currell, Physics in Medicine and Biology **53**, 5635 (2008).

[24] T. Ikeda, Y. Kanai, T. M. Kojima, Y. Iwai, T. Kambara, Y. Yamazaki, M. Hoshino, T. Nebiki, and T. Narusawa, Appl. Phys. Lett. **89**, 163502 (2006).

[25] S. W. Wilkins, T. E. Gureyev, D. Gao, A. Pogany, and A. W. Stevenson, Nature (London) **384**, 335 (1996).

[26] G. Schettino, M. Folkard, K. M. Prise, B. Vojnovic, K. D. Held, and B. D. Michael, Radiat. Res. **160**, 505 (2003).